

## Reflection of circumferential modes in a choked nozzle

By S. R. STOW, A. P. DOWLING AND T. P. HYNES

Department of Engineering, University of Cambridge, Cambridge CB2 1PZ, UK

(Received 11 October 2001 and in revised form 4 April 2002)

Small perturbations of a choked flow through a thin annular nozzle are investigated. Two cases are considered, corresponding to a ‘choked outlet’ and a ‘choked inlet’ respectively. For the first case, either an acoustic or entropy or vorticity wave is assumed to be travelling downstream towards the nozzle contraction. An asymptotic analysis for low frequency is used to find the reflected acoustic wave that is created. The boundary condition found by Marble & Candel (1977) for a compact choked nozzle is shown to apply to first order, even for circumferentially varying waves. The next-order correction can be expressed as an ‘effective length’ dependent on the mean flow (and hence the particular geometry of the nozzle) in a quantifiable way.

For the second case, an acoustic wave propagates upstream and is reflected from a convergent–divergent nozzle. A normal shock is assumed to be present. By considering the interaction of the shock’s position and flow perturbations, the reflected propagating waves are found for a compact nozzle. It is shown that a significant entropy disturbance is produced even when the shock is weak, and that for circumferential modes a vorticity wave is also present. Numerical calculations are conducted using a sample geometry and good agreement with the analysis is found at low frequency in both cases, and the range of validity of the asymptotic theory is determined.

---

### 1. Introduction

For choked outlet nozzles, Marble & Candel (1977) used a linear analysis to find a boundary condition that may be applied to perturbations. Their analysis was one-dimensional and the nozzle dimensions were assumed small compared with the shortest wavelength of the perturbed flow. The case of three-dimensional disturbances was investigated by Crocco & Sirignano (1967). However they assumed a similarity form which excludes the present thin annular geometry. For a compact choked inlet, attention has often been restricted to the case of a weak shock followed by smooth area increase. It has then been assumed (see for example Bloxsidge, Dowling & Langhorne 1988) that entropy perturbations are negligible leading to a simple reflection coefficient for plane acoustic waves. However in §4 we show that this assumption is incorrect. The main purpose of this work is to derive the appropriate boundary conditions for choked inlet and outlet nozzles when circumferentially varying modes are present and to test them by comparison between analytical and numerical results.

Lean premixed prevaporised (LPP) combustion can reduce  $\text{NO}_x$  emissions from gas turbines, but often leads to combustion instability. Acoustic waves produce fluctuations in heat release, for instance by perturbing the fuel–air ratio or flame shape. These heat fluctuations will in turn generate more acoustic waves and in some situations self-sustained oscillations can result. It is therefore important to be

able to predict resonant modes. To do this it is necessary to know the boundary conditions that apply at the inlet and outlet of the combustor. For short annular combustors, typical of aeroengines, circumferential modes must be considered but radial dependence is not important. The aim of this paper is to find the boundary conditions that apply to flow perturbations at a choked inlet and a choked outlet for a thin annular geometry.

In §2 we show that a linear disturbance in a straight annular duct can be thought of as a sum of acoustic, entropy and vorticity waves, with acoustic waves propagating both upstream and downstream, while entropy and vorticity disturbances convect with the mean flow. The equations presented there are required in forming the boundary conditions at the inlet and outlet of the nozzle in the subsequent sections.

Section 3 contains an asymptotic analysis of a choked outlet nozzle for low frequency. To first order the boundary condition for linear perturbations is found to agree with the Marble & Candel (1977) form for one-dimensional waves. Extending the boundary condition to second-order in compactness ratio (the product of wavenumber and nozzle length) the solution is found to depend on the mean flow. These boundary conditions are used to find the acoustic wave reflected when a downstream-propagating acoustic or a convected entropy or vorticity wave is incident on the nozzle. The results are expressed in the form of a reflection coefficient and an ‘effective length’ for the nozzle in terms of the mean flow.

In §4 we consider a compact convergent–divergent choked inlet nozzle with a normal shock in the divergent section. Now the interest is the determination of the downstream-travelling acoustic, vorticity and entropy waves produced by an incident upstream-propagating acoustic wave. We show that the boundary condition often used for a weak shock followed by smooth area increase is incorrect. We find new boundary conditions, that apply even without these assumptions, by considering the interaction of the shock position and the perturbed flow.

In §5 we present numerical results for a particular choked nozzle. Here the mean flow is assumed axisymmetric with no circumferential velocity and is calculated numerically using an Euler code. A linearized Euler technique is then used to calculate small perturbations to this flow. First, the reflected acoustic wave is found when a downstream-travelling acoustic, entropy or vorticity wave is incident on a choked exit nozzle. Secondly, the downstream-travelling acoustic wave produced by an upstream-propagating acoustic wave incident on a choked inlet nozzle is calculated. Good agreement is found between the numerical and analytical results.

## 2. Analysis for a straight annular duct

We consider the form of perturbations that can occur in the gap between two concentric cylinders. We first consider the general form, before investigating the case when the gap is narrow.

### 2.1. General form

Using cylindrical polar coordinates  $x$ ,  $r$  and  $\theta$ , we are interested in a straight annular duct of the form  $b \geq r \geq a \geq 0$ . The flow through this duct is assumed to be inviscid, with pressure  $p$ , density  $\rho$  and velocity  $\mathbf{u} = (u, v, w)$ . This flow is taken to be composed of a steady axial mean flow (denoted by bars) and a small perturbation (denoted by primes). These disturbances are assumed to have complex frequency  $\omega$  (i.e. the temporal dependence is of the form  $e^{i\omega t}$ ). We will restrict attention to real  $\omega$  (although extension to complex  $\omega$  is straightforward) and we may take  $\omega$  to be positive without

loss of generality. Also, the angular dependence of the perturbations is taken to be of the form  $e^{in\theta}$  (where  $n$  is a non-negative integer). Since  $\bar{v} = \bar{w} = 0$  for the uniform mean flow, the continuity equation for the perturbations becomes

$$i\omega\rho' + \bar{u}\frac{\partial\rho'}{\partial x} + \bar{\rho}\frac{\partial u'}{\partial x} + \bar{\rho}\frac{\partial(rv')}{\partial r} + in\bar{\rho}w' = 0, \quad (2.1)$$

and momentum equations for the perturbations become

$$i\omega\bar{\rho}u' + \bar{\rho}\bar{u}\frac{\partial u'}{\partial x} = -\frac{\partial p'}{\partial x}, \quad (2.2a)$$

$$i\omega\bar{\rho}v' + \bar{\rho}\bar{u}\frac{\partial v'}{\partial x} = -\frac{\partial p'}{\partial r}, \quad (2.2b)$$

$$i\omega\bar{\rho}w' + \bar{\rho}\bar{u}\frac{\partial w'}{\partial x} = -\frac{in}{r}p'. \quad (2.2c)$$

In the absence of viscosity and heat conduction the equation for entropy,  $S = c_v \log p/\rho^\gamma$ , is  $DS/Dt = 0$ . For the entropy perturbation,  $S' = c_v p'/\bar{p} - c_p \rho'/\bar{\rho}$ , this gives

$$i\omega S' + \bar{u}\frac{\partial S'}{\partial x} = 0 \quad (2.3)$$

(hence any variations in entropy at the inlet of the duct will be convected with the mean flow). The equation for vorticity,  $\xi$ , is  $D(\xi/\rho)/Dt = [(\xi/\rho) \cdot \nabla]\mathbf{u}$  (see Batchelor 1967). For the mean  $\bar{\xi} = \mathbf{0}$ , hence

$$i\omega\xi' + \bar{u}\frac{\partial\xi'}{\partial x} = 0 \quad (2.4)$$

(so vorticity variations are also convected).

If we first consider only isentropic irrotational disturbances ( $S' = 0$ ,  $\xi' = \mathbf{0}$ ), the perturbations are acoustic waves with the form

$$p' = A_\pm e^{i\omega t + in\theta + ik_\pm x} B_n(r), \quad (2.5a)$$

$$\rho' = \frac{1}{\bar{c}^2} A_\pm e^{i\omega t + in\theta + ik_\pm x} B_n(r), \quad (2.5b)$$

$$u' = -\frac{k_\pm}{\bar{\rho}\alpha_\pm} A_\pm e^{i\omega t + in\theta + ik_\pm x} B_n(r), \quad (2.5c)$$

$$v' = \frac{i}{\bar{\rho}\alpha_\pm} A_\pm e^{i\omega t + in\theta + ik_\pm x} \frac{dB_n}{dr}(r), \quad (2.5d)$$

$$w' = -\frac{n}{r\bar{\rho}\alpha_\pm} A_\pm e^{i\omega t + in\theta + ik_\pm x} B_n(r) \quad (2.5e)$$

(see Eversman 1994; Tyler & Sofrin 1962). Here  $\bar{c}$  is the mean speed of sound,

$$B_n(r) = \frac{dY_n}{dr}(\lambda_{n,m}b)J_n(\lambda_{n,m}r) - \frac{dJ_n}{dr}(\lambda_{n,m}b)Y_n(\lambda_{n,m}r), \quad \alpha_\pm = \omega + \bar{u}k_\pm$$

and

$$\bar{c}k_\pm = \frac{\bar{M}\omega \mp [\omega^2 - \bar{c}^2\lambda_{n,m}^2(1 - \bar{M}^2)]^{1/2}}{1 - \bar{M}^2}, \quad (2.6)$$

where  $\bar{M}$  is the mean Mach number (which is assumed to be less than unity) and  $\lambda_{n,m} \geq 0$  is the  $(m+1)$ th solution of

$$\frac{dJ_n(\lambda_{n,m}a)}{dr} \frac{dY_n(\lambda_{n,m}b)}{dr} = \frac{dJ_n(\lambda_{n,m}b)}{dr} \frac{dY_n(\lambda_{n,m}a)}{dr}$$

required to satisfy the rigid wall boundary condition on  $r = a$  and  $r = b$ . When  $\omega > \bar{c}\lambda_{n,m}(1-\bar{M}^2)^{1/2}$ ,  $A_+$  represents a downstream-propagating wave and  $A_-$  represents an upstream-propagating wave. For  $\omega < \bar{c}\lambda_{n,m}(1-\bar{M}^2)^{1/2}$  the waves are ‘cut off’;  $A_+$  then represents a downstream-decaying disturbance and  $A_-$  represents an upstream-decaying disturbance.†

We now consider an entropy disturbance by allowing  $S'$  to be non-zero (but keeping  $\xi' = \mathbf{0}$ ). Setting  $p' = 0$ , equations (2.1)–(2.4) imply the perturbations are an entropy wave of the form

$$\rho' = -\frac{1}{\bar{c}^2} A_E e^{i\omega t + in\theta + ik_0 x} E(r), \quad (2.7)$$

with  $p' = u' = v' = w' = 0$ , where  $k_0 = -\omega/\bar{u}$  and  $E(r)$  can be any function of  $r$ . (If we do not set  $p' = 0$ , we still have this entropy wave but the acoustic waves described above are also present.) Lastly we consider a vorticity disturbance, i.e.  $\xi'$  is non-zero (with  $S' = 0$ ). Taking  $p' = 0$  again, we find that  $\rho' = 0$  and  $\mathbf{u}' = (u^*(r), v^*(r), w^*(r)) e^{i\omega t + in\theta + ik_0 x}$ , where  $ik_0 u^* + (1/r)\partial(rv^*)/\partial r + (in/r)w^* = 0$ . There are two degrees of freedom here. The solution can be thought of as a sum of two types of vorticity wave, one where the radial velocity is zero and one where the circumferential velocity is zero. The first type has the form

$$u' = \frac{n}{\bar{\rho}\bar{c}} A_V e^{i\omega t + in\theta + ik_0 x} V(r), \quad (2.8a)$$

$$w' = -\frac{k_0 r}{\bar{\rho}\bar{c}} A_V e^{i\omega t + in\theta + ik_0 x} V(r), \quad (2.8b)$$

with  $p' = \rho' = v' = 0$ , whereas flow perturbations in the second type can be expressed as

$$u' = \frac{1}{\bar{\rho}\bar{c}r} A_W e^{i\omega t + in\theta + ik_0 x} \frac{dW}{dr}(r), \quad (2.9a)$$

$$v' = -\frac{ik_0}{\bar{\rho}\bar{c}r} A_W e^{i\omega t + in\theta + ik_0 x} W(r), \quad (2.9b)$$

with  $p' = \rho' = w' = 0$ . Here  $V(r)$  can be any function; however we must have  $W(a) = W(b) = 0$ . (Similar to the entropy case, if we do not set  $p' = 0$  we still have these vorticity waves but acoustic waves are also present.) Any flow perturbation can be expressed as a sum of the acoustic waves, entropy waves and vorticity waves described above.

## 2.2. Narrow annular gap

For the numerical scheme in §5 the equations above (including the Bessel functions  $B_n(r)$ ) are used when formulating boundary conditions. However for the analysis in §§3 and 4, a narrow annular gap assumption is used which simplifies the results. We write  $b = a(1 + \epsilon)$  and consider  $\epsilon \ll 1$ . Provided  $n \ll \epsilon^{-1}$  it can be shown that  $\lambda_{n,0} = n/R + O(\epsilon)^2$ , where  $R = \frac{1}{2}(a+b)$ , whereas  $\lambda_{n,m} = m\pi/(b-a) + O(\epsilon)$  for  $m \geq 1$  (see the Appendix). Hence if  $\omega < (1 - \bar{M}^2)^{1/2} \pi \bar{c}/(b-a)$  then the second and higher radial

† Note that the square root in (2.6) is taken to be a negative imaginary number in this case.

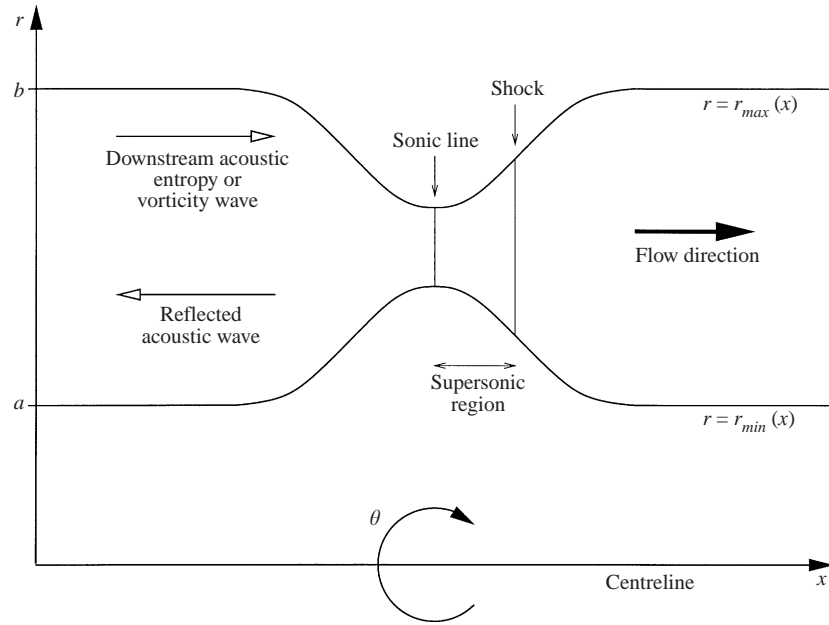


FIGURE 1. Schematic diagram of the choked outlet nozzle.

modes ( $m \geq 1$ ) will be cut off. If there is a source of such radial modes, then at a distance  $\Delta x$  away they will be negligible if say  $\omega^2 < [\pi\bar{c}/(b-a)]^2(1-M^2) - [3\bar{c}/(\Delta x)]^2$ , since the modes will be highly cut off and decay rapidly away from the source. Hence in such a situation we need only consider  $m = 0$ . Also it is not appropriate to consider  $n$  of order  $\epsilon^{-1}$ ; physically this is equivalent to saying that the circumferential wavelength should not be comparable with the radial gap.

### 3. Asymptotic analysis for a choked outlet nozzle

As well as the compact case, Marble & Candel (1977) also considered perturbations to choked flow when the wavelengths are comparable with the nozzle geometry. They assumed both the mean flow and the perturbations to be one-dimensional and approximated the mean velocity by a linear function. Here we extend their analysis by allowing the mean velocity to be a general function of  $x$  and considering circumferentially varying perturbations.

We consider an axisymmetric nozzle  $0 < x < x_{max}$ ,  $r_{min}(x) < r < r_{max}(x)$ , as shown schematically in figure 1. We suppose that there is a section at the inlet where the nozzle is simply the gap between two concentric cylinders as considered in §2, i.e.  $r_{min}(x) = a$ ,  $r_{max} = b$ . After this the cross-sectional area of the nozzle decreases to a throat at  $x = x_*$  before increasing again (see §5 for a particular example). The mean flow through the nozzle is assumed to be choked, with  $\bar{u} = \bar{u}(x)$  a known function (perhaps taken from steady numerical calculations as described in §5) and  $\bar{v} = \bar{w} = 0$ . Letting  $L$  be a typical axial length scale of the nozzle and writing  $X = x/L$ , we take the perturbed flow to be of the form

$$\frac{p'}{\gamma\bar{p}} = \hat{p}(X)e^{i\omega t + in\theta}, \quad \frac{\rho'}{\bar{\rho}} = \hat{\rho}(X)e^{i\omega t + in\theta}, \quad (3.1a)$$

$$\frac{u'}{\bar{u}} = \hat{u}(X)e^{i\omega t + in\theta}, \quad \frac{w'}{\bar{c}_{in}} = \hat{w}(X)e^{i\omega t + in\theta} \quad (3.1b)$$

(where subscript ‘in’ denotes values at the inlet) with  $v' = 0$ . We also make  $\omega$  non-dimensional by taking  $\Omega = L\omega/\bar{c}_*$  (where subscript ‘\*’ denotes values at the throat). We consider  $h(x) = r_{max}(x) - r_{min}(x)$  to be small compared to  $r_{max}(x)$  and hence take  $r \approx R = \frac{1}{2}(a + b)$ . Quantitatively, §2.2 implies that in order for the radial dependence of the perturbations to be negligible we need  $h$  to be sufficiently small that  $\Omega^2 < (\bar{c}/\bar{c}_*)^2[(\pi L/h)^2(1 - \bar{M}^2) - 9]$ . Section 2.2 also suggests that it is only appropriate to consider  $n \ll R/h$ . We use the narrow annular gap form of the Euler equations in which the continuity equation has the form

$$\frac{\partial}{\partial t}(\rho h) + \frac{\partial}{\partial x}(\rho u h) + \frac{1}{R} \frac{\partial}{\partial \theta}(\rho w h) = 0. \quad (3.2)$$

For linear perturbations this leads to

$$i\Omega \hat{\rho} + U \frac{d\hat{\rho}}{dX} + U \frac{d\hat{u}}{dX} + i\Omega_c \hat{w} = 0, \quad (3.3)$$

where  $\Omega_c = Ln\bar{c}_{in}/(R\bar{c}_*)$  and  $U(X) = \bar{u}(x)/\bar{c}_*$  (hence  $U(X_*) = 1$ ). The  $x$ -momentum equation for the narrow annular gap is

$$\frac{\partial u}{\partial t} + u \frac{\partial u}{\partial x} + \frac{w}{R} \frac{\partial u}{\partial \theta} + \frac{1}{\rho} \frac{\partial p}{\partial x} = 0. \quad (3.4)$$

The linearized form of this is

$$i\Omega \hat{u} + U \frac{d\hat{u}}{dX} + \frac{dU}{dX}(2\hat{u} + \hat{\rho}) + (\bar{c}^2/\bar{c}_*^2)U^{-1} \frac{d\hat{p}}{dX} + \gamma \hat{p} \frac{dU}{dX} L/(\bar{\rho} \bar{u} \bar{c}_*) = 0. \quad (3.5)$$

Substituting from the mean form of the axial-momentum equation,  $d\bar{p}/dx = -\bar{\rho} \bar{u} d\bar{u}/dx$ , and the steady-flow relationship,  $\bar{c}^2 = \frac{1}{2}(\gamma + 1)\bar{c}_*^2 - \frac{1}{2}(\gamma - 1)\bar{u}^2$ , this simplifies to

$$i\Omega \hat{u} + U \frac{d\hat{u}}{dX} + \frac{1}{2}[(\gamma + 1) - (\gamma - 1)U^2]U^{-1} \frac{d\hat{p}}{dX} + \frac{dU}{dX}(2\hat{u} + \hat{\rho} - \gamma \hat{p}) = 0. \quad (3.6)$$

The  $\theta$ -momentum equation here is

$$\frac{\partial w}{\partial t} + u \frac{\partial w}{\partial x} + \frac{w}{R} \frac{\partial w}{\partial \theta} + \frac{1}{\rho r} \frac{\partial p}{\partial \theta} = 0, \quad (3.7)$$

and linearizing this leads to

$$i\Omega \hat{w} + U \frac{d\hat{w}}{dX} + \frac{1}{2}i\Omega_c(\bar{c}_*/\bar{c}_{in})^2[(\gamma + 1) - (\gamma - 1)U^2]\hat{p} = 0. \quad (3.8)$$

The flow through the nozzle is assumed to be adiabatic. Therefore, upstream of any shocks, entropy is simply convected,

$$\frac{\partial S}{\partial t} + u \frac{\partial S}{\partial x} + \frac{w}{R} \frac{\partial S}{\partial \theta} = 0. \quad (3.9)$$

For linear disturbances this leads to

$$i\Omega(\hat{p} - \hat{\rho}) + U \left( \frac{d\hat{p}}{dX} - \frac{d\hat{\rho}}{dX} \right) = 0. \quad (3.10)$$

Our aim is to investigate the axial development of these linear perturbances and there is a particularly concise form for that development in terms of the perturbation in Mach number. To derive this form we multiply (3.6) by  $2U$  then subtract  $2U^{-1}$  times

(3.3) and  $U + U^{-1}$  times (3.10), giving

$$\begin{aligned} & i\Omega[U(2\hat{u} + \hat{\rho} - \hat{p}) - U^{-1}(\hat{p} + \hat{\rho} + 2\mu\hat{w})] \\ & + 2U\frac{dU}{dX}(2\hat{u} + \hat{\rho} - \gamma\hat{p}) + (U^2 - 1)\left(2\frac{d\hat{u}}{dX} + \frac{d\hat{\rho}}{dX} - \gamma\frac{d\hat{p}}{dX}\right) = 0, \end{aligned} \quad (3.11)$$

where  $\mu = \Omega_c/\Omega$ .

We now consider an asymptotic expansion for small  $\Omega$ ,

$$\hat{p} = \hat{p}_0 + i\Omega\hat{p}_1 + O(\Omega^2), \quad \hat{\rho} = \hat{\rho}_0 + i\Omega\hat{\rho}_1 + O(\Omega^2), \quad (3.12a)$$

$$\hat{u} = \hat{u}_0 + i\Omega\hat{u}_1 + O(\Omega^2), \quad \hat{w} = \hat{w}_0 + i\Omega\hat{w}_1 + O(\Omega^2). \quad (3.12b)$$

(Since we will be assuming that  $\bar{M}_{in}$  is small,  $\bar{c}_* \approx [2/(\gamma + 1)]^{1/2}\bar{c}_{in}$  and so  $\Omega$  being small is equivalent to the nozzle geometry being compact, i.e. short compared to  $\bar{c}_{in}/\omega$ .) Substituting (3.12) into (3.11) leads to

$$\frac{d}{dX}[(1 - U^2)(2\hat{u}_0 + \hat{\rho}_0 - \gamma\hat{p}_0)] = 0, \quad (3.13)$$

thus in order to avoid a singularity at the throat we must have that

$$2\hat{u}_0 + \hat{\rho}_0 - \gamma\hat{p}_0 = 0. \quad (3.14)$$

This is equivalent to Marble & Candel's boundary condition for a compact choked nozzle, obtained by considering the fractional mass flow (see Marble & Candel 1977). From (3.3) and (3.6)–(3.10) we also find that  $\hat{p}_0$ ,  $\hat{\rho}_0$ ,  $\hat{u}_0$  and  $\hat{w}_0$  are all constant. The expression  $2\hat{u} + \hat{\rho} - \gamma\hat{p}$  is proportional to the perturbation in the Mach number and so the boundary condition can simply be deduced from the fact that, for a time-independent disturbance, the Mach number remains purely a function of the cross-sectional area (provided the flow stays choked). To next order, (3.11) gives

$$\frac{d}{dX}[(1 - U^2)(2\hat{u}_1 + \hat{\rho}_1 - \gamma\hat{p}_1)] = U(2\hat{u}_0 + \hat{\rho}_0 - \hat{p}_0) - U^{-1}(\hat{p}_0 + \hat{\rho}_0 + 2\mu\hat{w}_0) \quad (3.15)$$

and hence

$$2\hat{u}_1 + \hat{\rho}_1 - \gamma\hat{p}_1 = \frac{\hat{p}_0 + \hat{\rho}_0 + 2\mu\hat{w}_0}{1 - U^2} \int_X^{X^*} U^{-1} dX - \frac{(\gamma - 1)\hat{p}_0}{1 - U^2} \int_X^{X^*} U dX. \quad (3.16)$$

At  $x = 0$  we therefore have the boundary condition

$$2\hat{u}(0) + \hat{\rho}(0) - \gamma\hat{p}(0) = i\Omega \left( \frac{\hat{p}_0 + \hat{\rho}_0 + 2\mu\hat{w}_0}{1 - U^2} I_1 - \frac{(\gamma - 1)\hat{p}_0}{1 - U^2} I_2 \right) + O(\Omega^2), \quad (3.17)$$

where  $I_1 = \int_0^{X^*} U^{-1} dX$  and  $I_2 = \int_0^{X^*} U dX$ .

An interesting question to ask is whether we can incorporate this  $O(\Omega)$  correction by simply approximating the nozzle by a straight duct, length  $l$  say, and applying the boundary condition  $2\hat{u} + \hat{\rho} - \gamma\hat{p} = 0$  at the end. This would give an 'effective length' for the nozzle which could be useful in applying acoustic models to industrial problems involving choked outlet pipes. We consider a flow along a straight duct  $0 < x < l$ ,  $r_{min}(0) < r < r_{max}(0)$ , such that the mean flow and perturbations at  $x = 0$  are the same as for the nozzle flow above. Denoting this new flow by superscript '\*',  $U^*(0) = U(0)$ ,  $\hat{p}^*(0) = \hat{p}(0)$ , etc. and since the duct is straight  $U^*(X) \equiv U(0)$ . In the same way as before,  $\hat{p}_0^*$ ,  $\hat{\rho}_0^*$ ,  $\hat{u}_0^*$  and  $\hat{w}_0^*$  are constant and so are equal to the values for

the nozzle flow. Equation (3.15) also applies to the new flow, leading to

$$[2\hat{u}_1^* + \hat{\rho}_1^* - \gamma\hat{p}_1^*]_0^{\hat{l}} = -\frac{\hat{p}_0 + \hat{\rho}_0 + 2\mu\hat{w}_0}{1 - U(0)^2} U(0)^{-1}\hat{l} + \frac{(\gamma - 1)\hat{p}_0}{1 - U(0)^2} U(0)\hat{l}, \quad (3.18)$$

where  $\hat{l}$  is the non-dimensional length  $l/L$ . Combining this with (3.17), we find that

$$\begin{aligned} & 2\hat{u}^*(\hat{l}) + \hat{\rho}^*(\hat{l}) - \gamma\hat{p}^*(\hat{l}) \\ &= i\Omega \left( \frac{\hat{p}_0 + \hat{\rho}_0 + 2\mu\hat{w}_0}{1 - U^2} [I_1 - U(0)^{-1}\hat{l}] - \frac{(\gamma - 1)\hat{p}_0}{1 - U^2} [I_2 - U(0)\hat{l}] \right), \end{aligned} \quad (3.19)$$

ignoring  $O(\Omega^2)$ . Hence the appropriate effective length is

$$l = \frac{(\hat{p}_0 + \hat{\rho}_0 + 2\mu\hat{w}_0)I_1 - (\gamma - 1)\hat{p}_0 I_2}{(\hat{p}_0 + \hat{\rho}_0 + 2\mu\hat{w}_0)U(0)^{-1} - (\gamma - 1)\hat{p}_0 U(0)} L, \quad (3.20)$$

giving the boundary condition

$$2\hat{u}^*(\hat{l}) + \hat{\rho}^*(\hat{l}) - \gamma\hat{p}^*(\hat{l}) = O(\Omega^2). \quad (3.21)$$

$U$  is small near the inlet and so we expect  $I_1$  to be much larger than  $I_2$ . Hence unless  $|\hat{p}_0 + \hat{\rho}_0 + 2\mu\hat{w}_0| \ll |\hat{p}_0|$ , a good approximation is given by

$$l = U(0)I_1 L = \int_0^{x^*} \frac{\bar{u}(0)}{\bar{u}(x)} dx, \quad (3.22)$$

which may be interpreted as the mean velocity at the inlet multiplied by the convection time to the throat. In the following sections we apply the above results to find the reflection coefficient for a downstream acoustic wave, an entropy wave or a vorticity wave at the inlet (see figure 1), and discuss the validity of (3.22).

### 3.1. Incident acoustic wave

We now consider the acoustic wave reflected as a result of a downstream-propagating acoustic wave incident on the nozzle (with no entropy or vorticity waves). Well upstream of the nozzle the mean flow will be approximately uniform and so (2.5) will apply.

We are assuming that the annular gap is sufficiently narrow that radial modes are highly cut off and can be ignored. Hence we should only consider  $m = 0$  with  $\lambda_{n,0} = n/R$  (see § 2.2). Also, since the gap is narrow we may set  $B_n(r) \equiv 1$ . Combining (2.5a) and (2.5c) gives the (pressure) reflection coefficient to be

$$\frac{A_-}{A_+} = -\frac{(\bar{c}k_+/\alpha_+)\hat{p}(0) + \bar{M}\hat{u}(0)}{(\bar{c}k_-/\alpha_-)\hat{p}(0) + \bar{M}\hat{u}(0)}, \quad (3.23)$$

where  $\bar{c}$  and  $\bar{M}$  denote the speed of sound and mean flow Mach number in the straight-walled annular region upstream of the nozzle. Equation (2.5) may also be applied to the straight-duct flow considered above when finding the effective length. Hence in a similar way

$$\frac{A_- e^{ik_- l}}{A_+ e^{ik_+ l}} = -\frac{(\bar{c}k_+/\alpha_+)\hat{p}^*(\hat{l}) + \bar{M}\hat{u}^*(\hat{l})}{(\bar{c}k_-/\alpha_-)\hat{p}^*(\hat{l}) + \bar{M}\hat{u}^*(\hat{l})}. \quad (3.24)$$

From (2.5),  $\hat{p}(0) = \hat{p}(0)$  and  $\hat{p}^*(\hat{l}) = \hat{p}^*(\hat{l})$ . Therefore (3.17) implies that  $\hat{u}(0) = \frac{1}{2}(\gamma - 1)\hat{p}(0)$  to  $O(\Omega)$ , whereas (3.21) gives  $\hat{u}^*(\hat{l}) = \frac{1}{2}(\gamma - 1)\hat{p}^*(\hat{l})$  to  $O(\Omega^2)$ . The reflection

coefficient is therefore

$$\begin{aligned} \frac{A_-}{A_+} &= -\frac{(\bar{c}k_+/\alpha_+) + \frac{1}{2}(\gamma-1)\bar{M}}{(\bar{c}k_-/\alpha_-) + \frac{1}{2}(\gamma-1)\bar{M}} + O(\Omega) \\ &= -\frac{(\bar{c}k_+/\alpha_+) + \frac{1}{2}(\gamma-1)\bar{M}}{(\bar{c}k_-/\alpha_-) + \frac{1}{2}(\gamma-1)\bar{M}} e^{i(k_+-k_-)l} + O(\Omega^2). \end{aligned} \quad (3.25)$$

For the simplified expression (3.22) for the effective length to be valid we required that  $|\hat{p}_0 + \hat{\rho}_0 + 2\mu\hat{w}_0| \ll |\hat{p}_0|$ . For the present case of purely acoustic waves, since  $\alpha_{\pm} = \omega + O(\bar{M})$  it follows from (2.5e) that  $\hat{w} = -\mu\hat{p} + O(\bar{M})$ . Hence the restriction becomes  $|1 - \mu^2| \ll 1$ , implying that for  $n = 0$  (3.22) is always valid whereas for non-zero  $n$  it is valid except close to the cut-off frequency (i.e.  $\mu \approx 1$ ).

### 3.2. Entropy wave

Since we are assuming  $r \approx R$  we should take  $B_n(r)$  and  $E(r)$  in (2.7) to be uniform, and for simplicity we take them to be equal to unity. We now define a reflection coefficient for the case of an entropy wave at the inlet to be  $A_-/A_E$ . (This is the reflection coefficient based on density.) Since  $A_+ = 0$ , (2.5) gives that  $\bar{M}\hat{u}^*(\hat{l}) = -(\bar{c}k_-/\alpha_-)\hat{p}^*(\hat{l})$  and so from (3.21),  $\bar{M}\hat{p}^*(\hat{l}) = [2(\bar{c}k_-/\alpha_-) + \gamma\bar{M}]\hat{p}^*(\hat{l})$  to  $O(\Omega^2)$ . From (2.5) and (2.7) we find that

$$\frac{A_-}{A_E} = \frac{\hat{p}^*(\hat{l})e^{-ik_-l}}{[\hat{p}^*(\hat{l}) - \hat{\rho}^*(\hat{l})]e^{-ik_0l}} = -\frac{\frac{1}{2}\bar{M}}{(\bar{c}k_-/\alpha_-) + \frac{1}{2}(\gamma-1)\bar{M}} e^{i(k_0-k_-)l} + O(\Omega^2). \quad (3.26)$$

Since  $\hat{\rho}/\hat{p} = O(\bar{M}^{-1})$ ,  $|\hat{p}_0 + \hat{\rho}_0 + 2\mu\hat{w}_0| \ll |\hat{p}_0|$  and so (3.22) is always valid for the entropy wave case.

### 3.3. Vorticity wave

As we are assuming a negligible radial dependence, we should only consider vorticity waves of the first type, as given by (2.8), and for simplicity we take  $V(r) \equiv B_n(r) \equiv 1$ . We define the reflection coefficient here to be  $(\bar{c}k_-/\alpha_-)A_-/(nA_V)$ . (This is the reflection coefficient based on axial velocity.) As in § 3.1,  $\hat{p}^*(\hat{l}) = \hat{p}^*(\hat{l})$  and  $\hat{u}^*(\hat{l}) = \frac{1}{2}(\gamma-1)\hat{p}^*(\hat{l}) + O(\Omega^2)$ . From (2.5) and (2.8) we have

$$\begin{aligned} \frac{\bar{c}k_-A_-}{n\alpha_-A_V} &= \frac{(\bar{c}k_-/\alpha_-)\hat{p}^*(\hat{l})e^{-ik_-l}}{[(\bar{c}k_-/\alpha_-)\hat{p}^*(\hat{l}) + \bar{M}\hat{u}^*(\hat{l})]e^{-ik_0l}} \\ &= \frac{\bar{c}k_-/\alpha_-}{(\bar{c}k_-/\alpha_-) + \frac{1}{2}(\gamma-1)\bar{M}} e^{i(k_0-k_-)l} + O(\Omega^2). \end{aligned} \quad (3.27)$$

From (2.5) and (2.8) we find that  $\hat{w}/\hat{p} = O(\bar{M}^{-1})$ , hence  $|\hat{p}_0 + \hat{\rho}_0 + 2\mu\hat{w}_0| \ll |\hat{p}_0|$  meaning that (3.22) is always valid for the vorticity wave case.

## 4. Analysis for a choked inlet nozzle

We now consider the reflected waves created when an upstream-propagating acoustic wave approaches a choked inlet nozzle (see figure 2). As before we assume that the nozzle is thin and annular, and that the cross-sectional area of the nozzle decreases to a throat before increasing again. At its outlet the nozzle is simply the gap between two concentric cylinders. We assume that a normal shock is present in the divergent

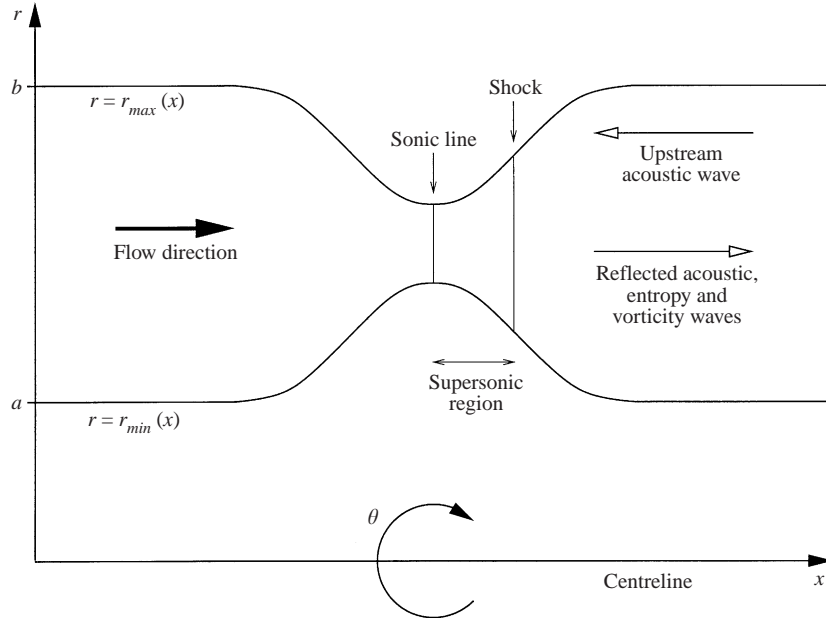


FIGURE 2. Schematic diagram of the choked inlet nozzle.

section of the nozzle. Since no upstream-propagating wave can travel across this shock and we assume that there are no inlet disturbances approaching the shock from upstream, there are no flow perturbations ahead of the shock. Behind the shock we assume there is the upstream-propagating acoustic wave and we wish to determine the downstream-travelling acoustic, vorticity and entropy waves generated in response to this incident disturbance. To find these downstream-travelling waves we must consider the interaction between the flow disturbances and the position of the shock. This is very similar to the work by Kuo & Dowling (1996) on oscillations of a supersonic jet impinging upon a flat plate. We take the shock to be at  $x = x_s = \bar{x}_s + x'_s$ . Since the perturbation in the shock position is caused by the upstream acoustic wave, it will have the form  $x'_s = \sigma e^{i\omega t + i n \theta}$ , where  $\sigma$  is a constant describing the amplitude of the shock displacement. Since we are considering linear perturbations, order  $\sigma^2$  is negligible. At the shock

$$c_1(x_s) = \bar{c}_1(\bar{x}_s) + x'_s \frac{d\bar{c}_1}{dx}(\bar{x}_s), \quad M_1(x_s) = \bar{M}_1(\bar{x}_s) + x'_s \frac{d\bar{M}_1}{dx}(\bar{x}_s), \quad (4.1)$$

where subscript '1' denotes values just ahead of the shock. (Here we have used the fact that the perturbations ahead of the shock are zero and so in particular  $c'_1(\bar{x}_s) = M'_1(\bar{x}_s) = 0$ .) Using subscript 'sh' to denote values in a frame of reference where the shock is stationary,

$$c_{1,sh} = c_1 = \bar{c}_1 + x'_s \frac{d\bar{c}_1}{dx}, \quad M_{1,sh} = M_1 - \frac{1}{c_1} \frac{dx_s}{dt} = \bar{M}_1 + x'_s \left( \frac{d\bar{M}_1}{dx} - \frac{i\omega}{\bar{c}_1} \right). \quad (4.2)$$

We assume that separation does not occur upstream of nor immediately after the shock. For the mean flow both ahead of and behind the shock, the one-dimensional flow equation shows that  $\bar{c}^2 = \bar{c}_0^2 [1 + \frac{1}{2}(\gamma - 1)\bar{M}^2]^{-1}$ , where subscript '0' denotes

stagnation values. Hence

$$\frac{d\bar{c}}{dx} = -\frac{\frac{1}{2}(\gamma-1)\bar{M}\bar{c}}{1+\frac{1}{2}(\gamma-1)\bar{M}^2} \frac{d\bar{M}}{dx}. \quad (4.3)$$

The usual Rankine–Hugoniot shock relations apply in the frame of reference where the shock is stationary and, in particular,

$$\frac{u_{1,sh}}{u_{2,sh}} = \frac{\frac{1}{2}(\gamma+1)M_{1,sh}^2}{1+\frac{1}{2}(\gamma-1)M_{1,sh}^2}, \quad (4.4)$$

where subscript ‘2’ denotes values just behind the shock; therefore

$$\begin{aligned} u_{2,sh} &= c_{1,sh} \frac{1+\frac{1}{2}(\gamma-1)M_{1,sh}^2}{\frac{1}{2}(\gamma+1)M_{1,sh}} \\ &= \bar{u}_2 - x'_s \frac{2\bar{c}_1}{(\gamma+1)\bar{M}_1^2} \left( \frac{d\bar{M}_1}{dx} - [1 - \frac{1}{2}(\gamma-1)\bar{M}_1^2] \frac{i\omega}{\bar{c}_1} \right) \end{aligned} \quad (4.5)$$

(cf. Kuo & Dowling 1996). Returning to the original frame of reference,

$$\begin{aligned} u_2 &= u_{2,sh} + \frac{dx_s}{dt} = \bar{u}_2 - x'_s \frac{2\bar{c}_1}{(\gamma+1)\bar{M}_1^2} \left( \frac{d\bar{M}_1}{dx} - (1+\bar{M}_1^2) \frac{i\omega}{\bar{c}_1} \right) \\ &= \bar{u}_2 + u'_2 + x'_s \frac{d\bar{u}_2}{dx} = \bar{u}_2 + u'_2 + x'_s \frac{\bar{c}_2}{1+\frac{1}{2}(\gamma-1)\bar{M}_2^2} \frac{d\bar{M}_2}{dx}. \end{aligned} \quad (4.6)$$

By considering the mass flux through the nozzle

$$\frac{1}{A} \frac{dA}{dx} = \frac{\bar{M}_1^2 - 1}{\bar{M}_1 [1 + \frac{1}{2}(\gamma-1)\bar{M}_1^2]} \frac{d\bar{M}_1}{dx} = \frac{\bar{M}_2^2 - 1}{\bar{M}_2 [1 + \frac{1}{2}(\gamma-1)\bar{M}_2^2]} \frac{d\bar{M}_2}{dx}, \quad (4.7)$$

where  $A$  is the cross-sectional area. Hence, defining  $\hat{u}$  as before, just after the shock we have

$$\hat{u} = -\frac{\sigma}{\bar{M}_1 [1 + \frac{1}{2}(\gamma-1)\bar{M}_1^2]} \left[ \left( 1 + \frac{\bar{M}_1^2 - 1}{\bar{M}_2^2 - 1} \right) \frac{d\bar{M}_1}{dx} - (1 + \bar{M}_1^2) \frac{i\omega}{\bar{c}_1} \right]. \quad (4.8)$$

In a similar way we also find that just after the shock

$$\begin{aligned} \hat{p} &= \frac{\sigma}{\bar{M}_1 [1 + \frac{1}{2}(\gamma-1)\bar{M}_1^2]} \left[ \left( \bar{M}_1^2 \frac{\gamma+3-2\bar{M}_1^2}{2\gamma\bar{M}_1^2 - (\gamma-1)} + \bar{M}_2^2 \frac{\bar{M}_1^2 - 1}{\bar{M}_2^2 - 1} \right) \right. \\ &\quad \left. \times \frac{d\bar{M}_1}{dx} - \frac{2\bar{M}_1^2 [2 + (\gamma-1)\bar{M}_1^2]}{2\gamma\bar{M}_1^2 - (\gamma-1)} \frac{i\omega}{\bar{c}_1} \right], \end{aligned} \quad (4.9)$$

$$\hat{p} = \frac{\sigma}{\bar{M}_1 [1 + \frac{1}{2}(\gamma-1)\bar{M}_1^2]} \left[ \left( 2 - \bar{M}_1^2 + \bar{M}_2^2 \frac{\bar{M}_1^2 - 1}{\bar{M}_2^2 - 1} \right) \frac{d\bar{M}_1}{dx} - 2 \frac{i\omega}{\bar{c}_1} \right] \quad (4.10)$$

and  $w' = 0$ . Using a similar procedure to that above, Culick & Rogers (1983) considered the interaction of a shock in a choked inlet with one-dimensional flow perturbations. They only calculated the admittance immediately after the shock and hence did not need to consider whether an entropy perturbation is present. They also did not investigate the effect of the area increase following the shock. The admittance

function calculated using (4.8) and (4.9) is equivalent to their result (except for a typographical error†).

In the following we will assume that the nozzle is compact and hence ignore the  $\omega/\bar{c}_1$  terms above. (This is equivalent to considering only the first-order terms in an expansion similar to (3.12).) We now consider three fluxes along the nozzle: the mass flux,  $m = A\rho u$ , the angular-momentum flux,  $f_\theta = Rmw$ , and the energy flux,  $e = A\gamma pu/(\gamma-1) + m(\frac{1}{2}u^2 + \frac{1}{2}w^2)$ . By considering the perturbations of these we find that  $m' = \bar{m}(\hat{\rho} + \hat{u})$ ,  $f'_\theta = R\bar{m}w'$  and  $(\gamma-1)e' = [1 + \frac{1}{2}(\gamma-1)\bar{M}^2]\bar{c}^2 m' + \bar{c}^2 \bar{m}[\gamma\hat{p} - \hat{\rho} + (\gamma-1)\bar{M}^2\hat{u}]$ . Applying (4.8)–(4.10) and using the shock relation

$$\bar{M}_2^2 = \frac{1 + \frac{1}{2}(\gamma-1)\bar{M}_1^2}{\gamma\bar{M}_1^2 - \frac{1}{2}(\gamma-1)} \quad (4.11)$$

give that  $m' = f'_\theta = e' = 0$  just after the shock.

We must now consider the effects of the increase in nozzle cross-sectional area between the shock and the straight outlet. By considering a thin sector of the nozzle, it can be seen that the fluxes  $m$ ,  $f_\theta$  and  $e$  are all conserved across this increase in area, assuming it is compact. Hence  $m' = f'_\theta = e' = 0$  also at the outlet, and so  $\hat{\rho} + \hat{u} = w' = \gamma\hat{p} - \hat{\rho} + (\gamma-1)\bar{M}^2\hat{u} = 0$ . We now use (2.5), (2.7) and (2.8) to find the reflected downstream acoustic wave, entropy wave and vorticity wave created by the upstream acoustic wave. Since  $\gamma\hat{p} - [1 + (\gamma-1)\bar{M}^2]\hat{\rho} = 0$ , the entropy wave is given by

$$A_E = \frac{(\gamma-1)(1-\bar{M}^2)}{1 + (\gamma-1)\bar{M}^2}(A_- + A_+), \quad (4.12)$$

and using  $w' = 0$ , the vorticity wave is given by

$$A_V = -\frac{n\bar{c}}{R^2k_0} \left( \frac{A_-}{\alpha_-} + \frac{A_+}{\alpha_+} \right). \quad (4.13)$$

Here  $R$  is the mean radius at the outlet, and as before we have taken  $E(r) = V(r) = B_n(r) = 1$  and  $m = 0$  with  $\lambda_{n,0} = n/R$ . Also, from  $\gamma\hat{p} + [1 + (\gamma-1)\bar{M}^2]\hat{u} = 0$  we find that the reflection coefficient for the downstream acoustic wave is

$$\frac{A_+}{A_-} = \frac{(\bar{c}k_-/\alpha_-) - [n^2\bar{c}/(R^2k_0\alpha_-)] - \gamma\bar{M}/[1 + (\gamma-1)\bar{M}^2]}{(\bar{c}k_+/\alpha_+) - [n^2\bar{c}/(R^2k_0\alpha_+)] - \gamma\bar{M}/[1 + (\gamma-1)\bar{M}^2]}. \quad (4.14)$$

As well as the reflected acoustic wave, we see that an entropy wave is created, and for non-zero  $n$  there is also a vorticity wave.

#### 4.1. Weak shock and smooth area increase

We now consider the special case of a weak shock followed by a smooth area increase. We therefore consider a shock for which  $\bar{M}_1^2 = 1 + \epsilon$  with  $0 < \epsilon \ll 1$  (i.e. the shock is weak). From the Rankine–Hugoniot shock relations, the mean entropy increase across the shock is

$$\bar{S}_2 - \bar{S}_1 = c_v \frac{2\gamma(\gamma-1)}{3(\gamma+1)^2} \epsilon^3 + \dots = c_v \frac{(\gamma^2-1)}{12\gamma^2} \left( \frac{\bar{p}_2 - \bar{p}_1}{\bar{p}_1} \right)^3 + \dots, \quad (4.15)$$

where  $S$  denotes the entropy and  $c_v$  is the specific heat at constant volume. Hence the mean entropy produced by the shock is negligible. A quasi-steady approach suggests

† In equation (39) on p. 1386 of Culick & Rogers (1983),  $\bar{p}_1/\bar{p}_2$  should read  $\bar{p}_1\bar{a}_2/(\bar{p}_2\bar{a}_1)$ .

that the entropy perturbation just after the shock will be

$$S'_2 = c_p \frac{(\gamma^2 - 1) p'_2 (\bar{p}_2 - \bar{p}_1)^2}{4\gamma^2 \bar{p}_1^3} + \dots = c_p \frac{\gamma - 1}{\gamma + 1} \epsilon^2 \hat{p}_2 + \dots, \quad (4.16)$$

where  $c_p$  is the specific heat at constant pressure (however we show below that this is not correct in the stationary frame of reference). It therefore appears that the entropy perturbation is also negligible. If the area increase is smooth, very little entropy will be produced for the mean flow and for the perturbations. Conservation of mass across the shock and along the area increase then gives  $m' = 0$  at the nozzle outlet. This would imply that  $\hat{p} + \hat{u} = 0$ , leading to a reflection coefficient for the downstream acoustic wave of

$$\frac{A_+}{A_-} = \frac{1 - \bar{M}}{1 + \bar{M}} \quad (4.17)$$

for  $n = 0$ , a form that has often been used in the literature (see for example Bloxside *et al.* 1988). However, for  $n = 0$ , (4.14) gives

$$\frac{A_+}{A_-} = \frac{1 - \gamma \bar{M} + (\gamma - 1) \bar{M}^2}{1 + \gamma \bar{M} + (\gamma - 1) \bar{M}^2} \quad (4.18)$$

and an apparent inconsistency. We are forced to conclude that the assumption of negligible entropy perturbations must be incorrect.

To explain this apparent discrepancy we return to the approach used to derive equations (4.8)–(4.10). In a frame of reference where the shock is stationary, just downstream of the shock we have

$$\hat{u}_{2,sh} = -\beta, \quad \hat{p}_{2,sh} = \beta, \quad (4.19a)$$

$$\hat{p}_{2,sh} = \beta, \quad S'_{2,sh} = c_p \frac{2(\gamma - 1)}{\gamma + 1} \beta \epsilon^2 \quad (4.19b)$$

to first order in  $\epsilon$ , where  $\beta = 2\sigma(d\bar{M}_1/dx)/(\gamma + 1)$ . This agrees with the relative orders of magnitude suggested by (4.16). However, after reverting to the nozzle-fixed frame of reference we find that to leading order

$$\hat{u}_2 = \frac{2\gamma}{\gamma + 1} \beta \epsilon, \quad \hat{p}_2 = -\frac{2\gamma}{\gamma + 1} \beta \epsilon, \quad (4.20a)$$

$$\hat{p}_2 = -\frac{2\gamma}{\gamma + 1} \beta \epsilon, \quad S'_2 = c_p \frac{2(\gamma - 1)}{\gamma + 1} \beta \epsilon^2. \quad (4.20b)$$

After the area increase we have  $m' = e' = 0$  as before, but since the area change is smooth we also have conservation of entropy. This leads to

$$\hat{u} = \frac{2\gamma}{(\gamma + 1)(1 - \bar{M}^2)} \beta \epsilon^2, \quad \hat{p} = -\frac{2 - 2(\gamma - 1)\bar{M}^2}{(\gamma + 1)(1 - \bar{M}^2)} \beta \epsilon^2, \quad (4.21a)$$

$$\hat{p} = -\frac{2\gamma}{(\gamma + 1)(1 - \bar{M}^2)} \beta \epsilon^2, \quad S' = c_p \frac{2(\gamma - 1)}{\gamma + 1} \beta \epsilon^2 \quad (4.21b)$$

to leading order at the nozzle outlet. The flow perturbations just after the shock are much smaller in a stationary frame of reference than in a frame of reference moving with the shock. Unless  $\bar{M} \approx 1$  at the nozzle outlet, these flow perturbations are much smaller still (by a factor  $\epsilon$ ) after the area increase and are then comparable with the entropy disturbance. In fact from (4.12) and (4.14) it can be seen that even for  $\bar{M} \approx 1$

the entropy disturbance is comparable with the reflected acoustic wave. This therefore explains why the entropy perturbations created by the shock should not be neglected.

## 5. Numerical results

In this section, we test the results of §§ 3 and 4 numerically to investigate the range of validity of the asymptotic solutions. We consider a particular geometry of nozzle: near its inlet and outlet the nozzle is taken to be the gap between two concentric cylinders, specifically  $r_{min}(x) = a$ ,  $r_{max} = b$  for  $0 < x < \frac{1}{4}x_{max}$  and  $\frac{3}{4}x_{max} < x < x_{max}$ . Between these sections the cross-sectional area of the nozzle decreases to a throat at  $x = \frac{1}{2}x_{max}$ ; we take  $r_{min}(x) = a + \frac{1}{2}d[1 + \cos(4\pi x/x_{max})]$  and  $r_{max}(x) = b - \frac{1}{2}d[1 + \cos(4\pi x/x_{max})]$  for  $\frac{1}{4}x_{max} < x < \frac{3}{4}x_{max}$ . This is shown schematically in figures 1 and 2. In the numerical calculations the values  $a = 0.18$  m,  $b = 0.27$  m and  $d = 0.032$  m were used and the inlet stagnation pressure and stagnation temperature were taken to be 216 kPa and 986 K respectively. (These values are based on the outlet of an aeroengine combustion chamber at idle conditions.) The value of  $x_{max}$  was chosen to aid comparison with the analytical results (this is discussed below). Typically  $x_{max} = 0.2$  m was used for the choked outlet case, and  $x_{max} = 0.4$  m for the choked inlet.

The mean flow is assumed axisymmetric with  $\bar{w} = 0$  and hence may be calculated numerically on a two-dimensional grid. The numerical technique used involves a finite volume method by which the imbalance of fluxes into the cells is used to update nodal values of flow variables in a time-stepping manner until convergence to a steady solution is obtained. Fluxes across cell boundaries are formed from nodal values in a centred manner, implying a second-order-accurate formulation. The time-stepping algorithm is based on an explicit method due to Denton (2002) which requires a very low level of explicit numerical viscosity. The effect of this on the converged solution is reduced further by the use of a deferred correction technique. The stagnation pressure and stagnation temperature were fixed at the inlet (using the values stated above) with  $\bar{v}$  set to be zero. At the outlet the (static) pressure was specified (typically 100 kPa). Some mean-flow results are shown in figure 3. Here the average Mach number at each axial location is plotted. Generally, a grid of 80 cells in the axial direction by 20 cells in the radial direction was found to be sufficient. The solid, dashed and dotted lines denotes outlet pressures of 100 kPa, 150 kPa and 200 kPa, respectively. In the first two cases  $x_{max}$  was taken to be 0.2 m, whereas  $x_{max} = 0.4$  m for other case. In these cases, ahead of the shock the mean flow was found to vary little with  $r$ . Downstream of the shock there was large radial variation, except for the third case.

The linearly perturbed flow was calculated in a similar way. A linearized Euler method was used with the mean flow taken from the calculations described above. The angular dependence of the perturbations is taken to be of the form  $e^{in\theta}$  and so the solution may be calculated on the same two-dimensional grid as the mean flow, even though the perturbed velocity is three-dimensional. The disturbances are assumed to have complex frequency  $\omega$  and so the complex amplitudes of the solution can be found using pseudo-time stepping. The choked outlet and choked inlet cases differ in the boundary conditions applied at  $x = 0$  and  $x = x_{max}$ , and are discussed in §§ 5.1 and 5.2, respectively.

### 5.1. Choked outlet nozzle

Incident on the nozzle from upstream we impose either a downstream-travelling acoustic wave, entropy wave or vorticity wave. These three cases are considered separately below.

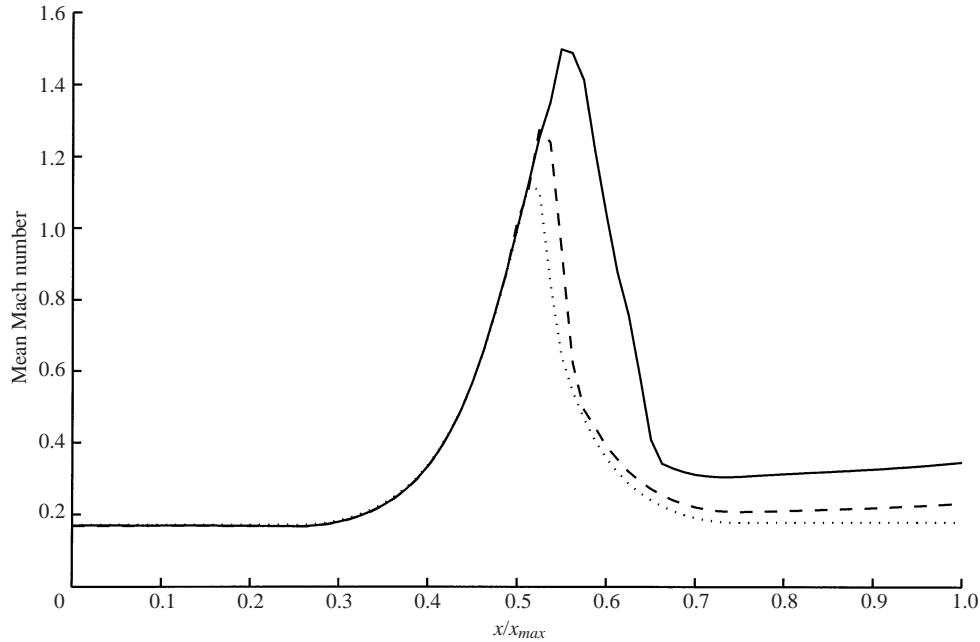


FIGURE 3. Mach number of the mean flow averaged over  $r$ , using a grid of  $80 \times 20$  cells. For the solid and dashed lines,  $x_{max} = 0.2$  m with the outlet pressure set at 100 kPa and 150 kPa, respectively. The dotted line represents an outlet pressure of 200 kPa with  $x_{max} = 0.4$  m.

### 5.1.1. Downstream acoustic wave

Provided the inlet is chosen to be sufficiently far upstream of the nozzle, the mean flow will be uniform there and so linear perturbations will be a superposition of disturbances of the form shown in (2.5). At the inlet we impose a downstream-propagating acoustic wave with  $m = 0$ , and no entropy or vorticity disturbances. This will potentially create reflected acoustic waves of all radial modes, not just  $m = 0$ . Hence the full perturbation at the inlet is given by the '+' form of (2.5) with  $m = 0$  added to the '-' form summed over  $m$ . For the range of frequencies that are considered in these test cases, the radial harmonics corresponding to  $m > 0$  are highly cut off. The resulting rapid exponential decay in the upstream direction of the '-' form (which can be viewed as exponential growth in the downstream direction) and the corresponding behaviour of the '+' form leads to a poorly conditioned problem if the upstream boundary conditions include  $m > 0$ . In order to maintain a well-conditioned problem, we have assumed that any  $m > 0$  modes generated at the downstream end will have decayed to zero at the upstream end. The boundary condition there is thus imposed only in terms of the  $m = 0$  radial mode. This leads to the following numerical scheme: at each pseudo-time step the solution at  $x = 0$  was decomposed to find  $A_+$  and  $A_-$  (see below), the solution at  $x = 0$  was then recalculated using (2.5) with this value of  $A_-$  but setting  $A_+$  to be a fixed constant and ignoring  $m > 0$ . The reflection coefficient is then given by  $A_-/A_+$  for the converged solution. The decomposition to find  $A_+$  and  $A_-$  at the inlet is as follows: we multiply the pressure perturbation at  $x = 0$  by  $rB_n(r; m = 0)/\int_a^b rB_n(r; m = 0)^2 dr$  and numerically integrate across the radius. This procedure gives the  $B_n(r; m = 0)$ -component of pressure perturbation, which we denote by  $p'_0$ . The  $B_n(r; m = 0)$ -component of velocity perturbation,  $u'_0$ , is found in the same way. From equation (2.5),  $p'_0 = A_+ + A_-$  and  $u'_0 = -k_+A_+/(\bar{\rho}\alpha_+) - k_-A_-/(\bar{\rho}\alpha_-)$ .

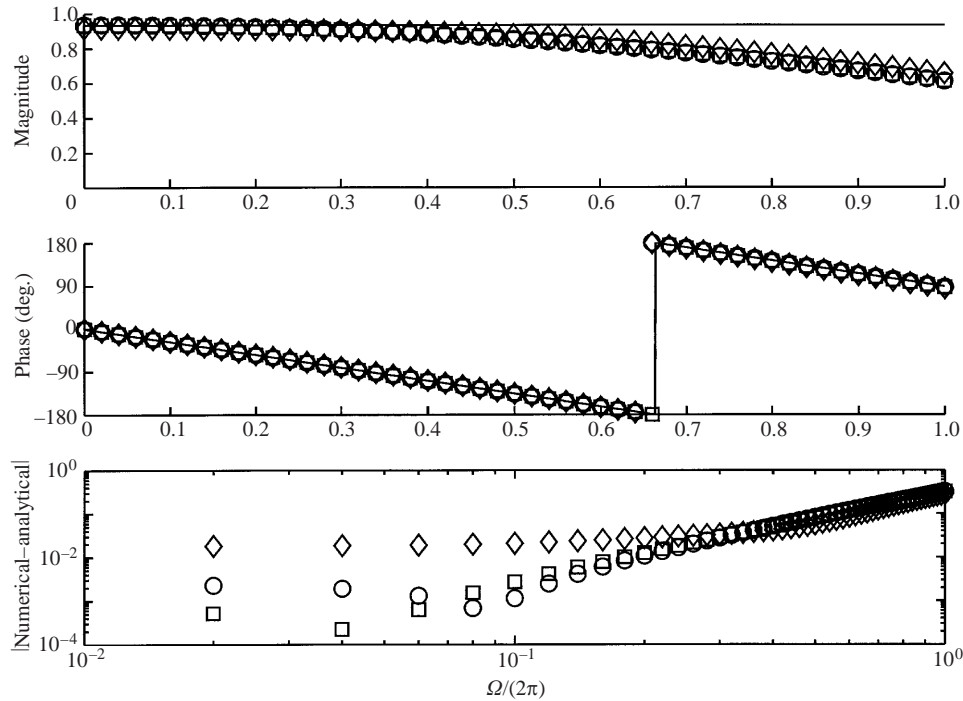


FIGURE 4. Magnitude and phase of the reflection coefficient for a choked nozzle with a downstream acoustic wave at the inlet ( $n = 0$ ). The circles, squares and diamonds represent numerical results for outlet pressures of 100, 150 and 200 kPa respectively. For the circles and squares  $x_{max} = 0.2$  m, whereas  $x_{max} = 0.4$  m for the diamonds. The solid lines denote analytical results. The absolute difference between the numerical and analytical results is also shown.

(Note that the factors of  $e^{i\omega t + in\theta}$  in (2.5) are already assumed by the numerical solution.) These two equations are then solved to find  $A_+$  and  $A_-$ .

The appropriate boundary condition at the nozzle exit is that all waves are outward propagating. Since we are interested in short nozzles and a choked mean flow, separation is likely, owing to the high speed and the abrupt area expansion. Hence (2.5) may not be a good approximation at the nozzle outlet. But as there will be a region of supersonic flow just downstream of the throat, where all disturbances will be carried downstream, we would expect that the perturbed flow at the nozzle inlet is in fact independent of the flow in the divergent section of the choked nozzle. Numerically this was indeed found to be the case. Typically, the boundary condition used at  $x = x_{max}$  was simply to reduce all perturbed flow variables by a half at each time step.

Figure 4 shows results for the magnitude and phase of the plane-wave ( $n = 0$ ) reflection coefficient for different mean flows (corresponding to the three cases shown in figure 3). (In this and the subsequent figures, the value of  $L$  used in the definition of  $\Omega$  is  $x_{max}$ .) For the circles and squares the outlet pressure was 100 kPa and 150 kPa, respectively, with  $x_{max} = 0.2$  m. For comparison with the results in § 5.2, the diamonds represent an outlet pressure of 200 kPa with  $x_{max} = 0.4$  m. A grid of  $80 \times 20$  cells was used for each case and all other parameters were as stated at the beginning of § 5. We see that the results vary very little despite the large range in outlet pressure; for all remaining figures in § 5.1 the value 100 kPa was used. Numerical calculations of (3.22) give  $l \approx 0.081$  m. Hence in this and subsequent figures, the solid lines

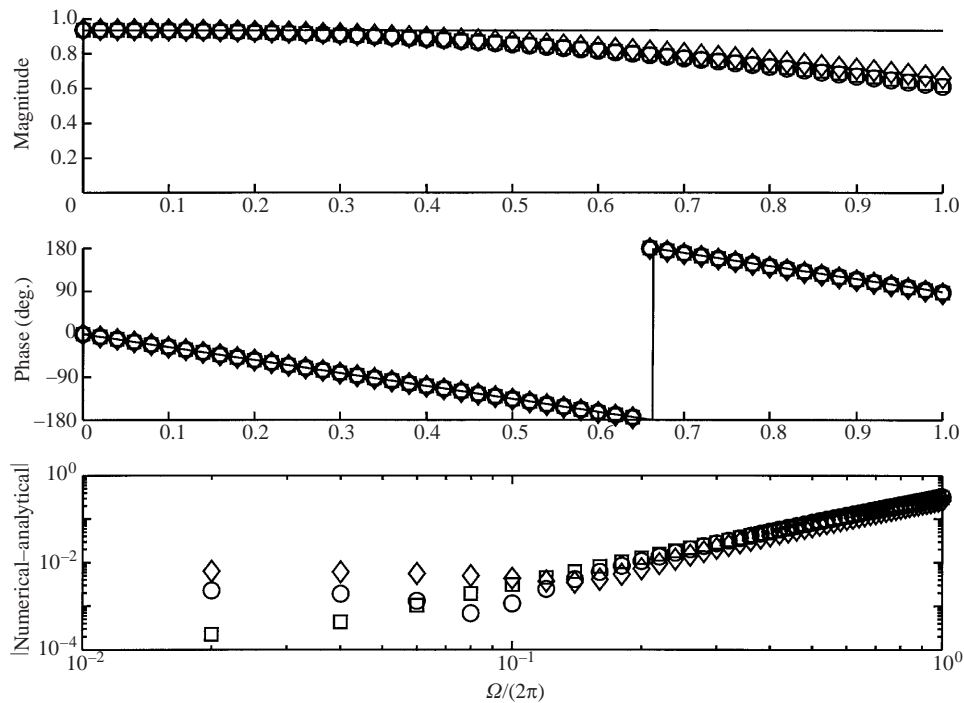


FIGURE 5. Magnitude and phase of the reflection coefficient for a choked nozzle with a downstream acoustic wave at the inlet ( $n = 0$ ). The circles and squares represent numerical results for grids of  $80 \times 20$  and  $160 \times 40$  cells, respectively, with  $x_{max} = 0.2$  m. The diamonds represent numerical results for a grid of  $80 \times 20$  cells with  $x_{max} = 0.4$  m. The solid lines denote analytical results. The absolute difference between the numerical and analytical results is also shown.

represent Marble & Candel's boundary condition with an effective length of 0.08 m. (The absolute difference between the numerical results and this analytical result is also shown in the figure.) We see that there is very good agreement between the numerical results and analysis, particularly at lower frequencies. The frequency of combustion instabilities in gas turbines is typically less than 1 kHz. A typical length scale over which choking occurs at the turbine inlet is 0.04 m, suggesting  $L = 0.08$  m is a suitable value for comparing the nozzle geometry used here with a real engine. Taking the temperature to be around 1800 K, this implies that  $\Omega/(2\pi)$  is typically less than 0.1 in applications;  $h(x)$  close to the turbine inlet is typically around 0.08 m hence the condition  $\Omega^2 < (\bar{c}/\bar{c}_*)^2 [(\pi L/h)^2 (1 - \bar{M}^2) - 9]$  for the narrow annular gap assumption to be valid becomes  $\Omega/(2\pi) < 0.16$ .

Figure 5 shows results for the reflection coefficient with  $n = 0$  to demonstrate grid dependence and the effect of  $x_{max}$ . The circles are the same as in the previous figure, whereas the squares are for a grid of  $160 \times 40$  cells. There is little difference between these results, showing that a grid of  $80 \times 20$  cells is sufficient. The diamonds denote results for  $80 \times 20$  cells but with  $x_{max} = 0.4$  m. For fixed  $\Omega$  there is again little difference between the results; however at fixed frequency agreement with the analysis is better for  $x_{max} = 0.2$  m. The gradient of the points in the plot of the absolute difference between the analytical and numerical results appears to indicate that for  $\Omega/(2\pi)$  above about 0.1 the discrepancy is due an error in the analysis of order  $\Omega^2$ , as expected since the analysis is only to order  $\Omega$ . For lower frequencies the discrepancy appears to be due to numerical errors that are approximately independent of frequency, these

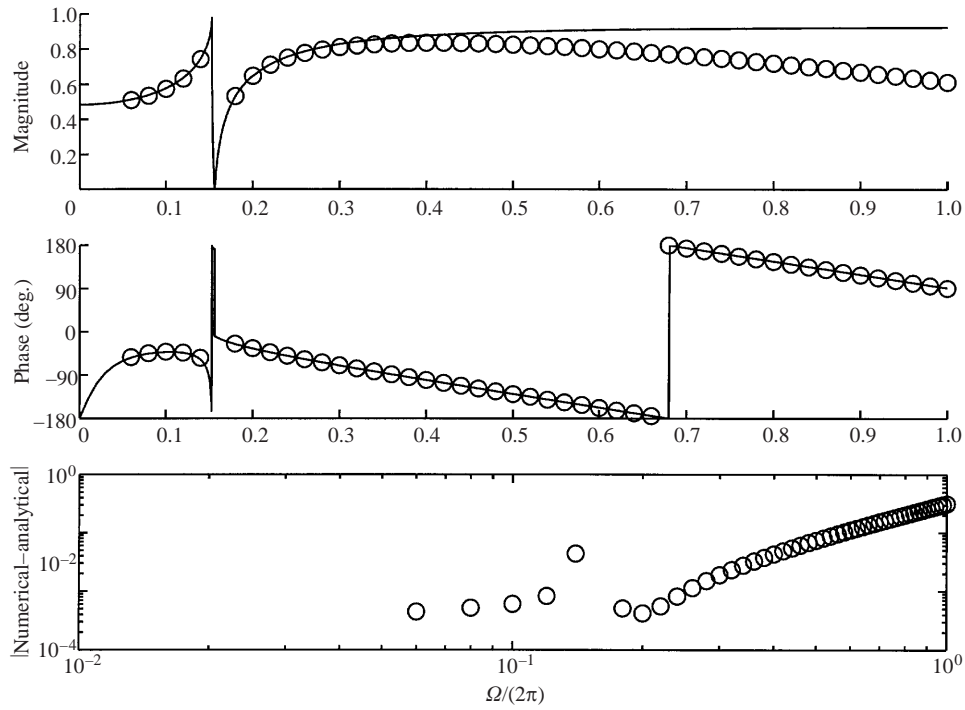


FIGURE 6. Magnitude and phase of the reflection coefficient for a choked nozzle with a downstream acoustic wave at the inlet ( $n = 1$ ). The circles and solid lines denote numerical and analytical results respectively. The absolute difference between the numerical and analytical results is also shown.

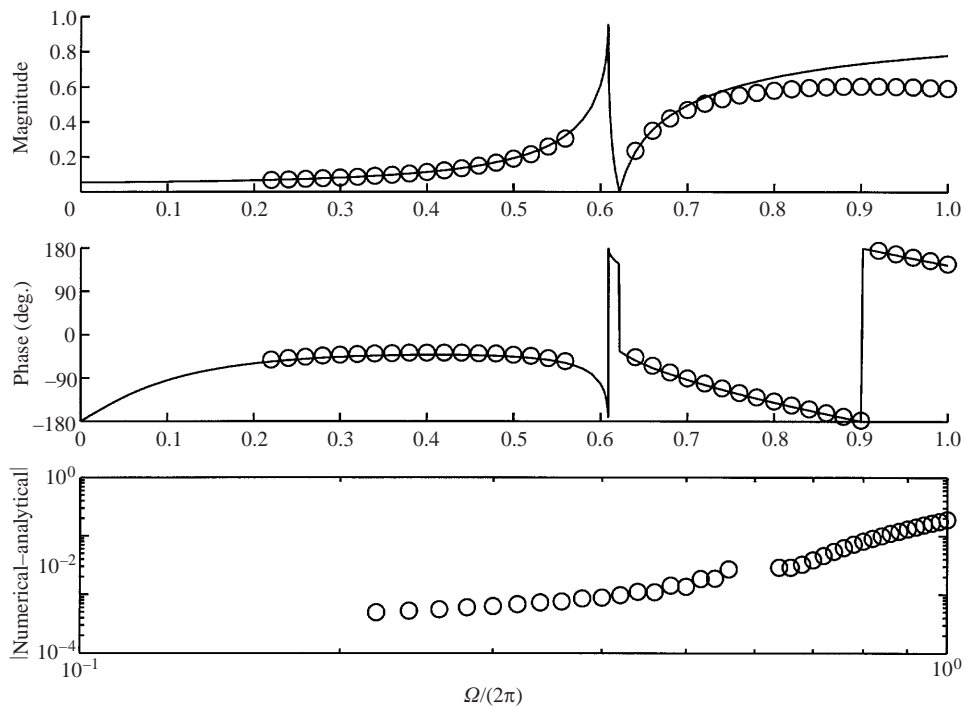


FIGURE 7. As figure 6 but for  $n = 4$ .

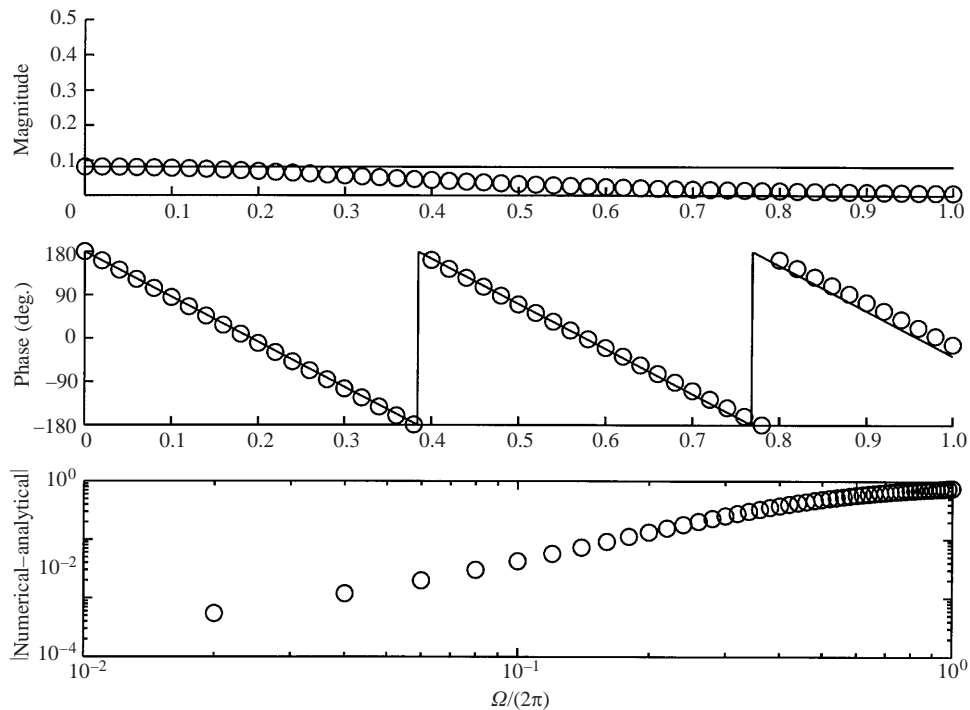


FIGURE 8. Magnitude and phase of the reflection coefficient for a choked nozzle with an entropy wave at the inlet ( $n = 0$ ). The circles and solid lines denote numerical and analytical results respectively. The absolute difference between the numerical and analytical results is also shown.

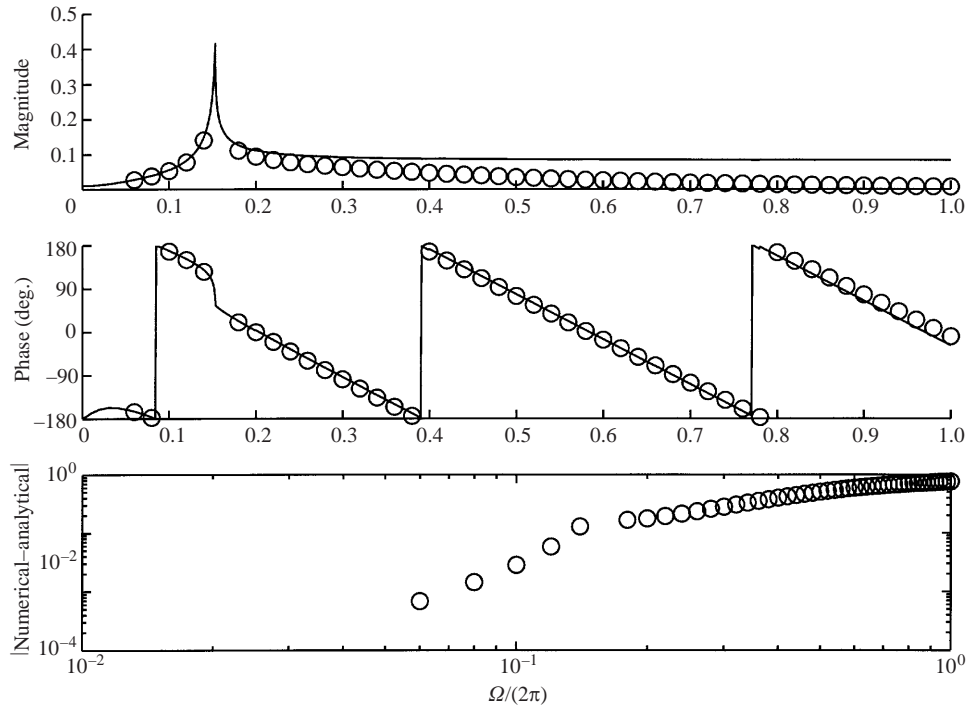
being smaller for the finer grid. In the subsequent figures in § 5.1,  $80 \times 20$  cells were used with  $x_{max} = 0.2$  m.

Numerical results for the reflection coefficient (3.25) for the first azimuthal mode ( $n = 1$ ) are shown in figure 6. (Numerical difficulties were met at very low frequencies and the results are shown for  $\Omega/(2\pi) \geq 0.06$ .) The cutoff frequency is 440 Hz, equivalent to  $\Omega/(2\pi) = 0.15$ . Results for  $n = 4$  are shown in figure 7. (Here results are shown for  $\Omega/(2\pi) \geq 0.22$  due to numerical difficulties at very low frequencies.) The cutoff frequency is now 1750 Hz corresponding to  $\Omega/(2\pi) = 0.61$ . For both these circumferential-mode cases there is again good agreement with the analysis. In real annular gas turbines, the circumferential wavenumber of combustion instabilities is low, for example Seume *et al.* (1997) report finding modes with  $n = 2$  and  $n = 4$  in tests of a large industrial combustor.

### 5.1.2. Entropy wave

The reflection coefficient for an incident entropy wave was calculated in a similar way. At each pseudo-time step in the numerical scheme, we decompose the solution at  $x = 0$  to find  $A_+$  and  $A_-$ . We then recalculate the solution at  $x = 0$  using (2.5) with  $A_+$  set to zero and ignoring the higher-order radial modes. We also add an entropy wave at  $x = 0$  using (2.7) with  $A_E$  set to be a fixed constant. For simplicity and comparison with § 3 we take  $E(r) = B_n(r)$ . The reflection coefficient is then  $A_-/A_E$  for the converged solution. The outlet boundary condition is treated in the same way as before.

Figure 8 shows results for the magnitude and phase of the reflection coefficient

FIGURE 9. As figure 8 but for  $n = 1$ .

with  $n = 0$ . (The absolute difference between numerical and analytical results is also shown.) Equivalent results for  $n = 1$  are shown in figure 9. In both cases, correspondence with the analysis is very good at low frequency but becomes poor as the frequency increases. The agreement at higher frequencies is much worse here than for the case of a downstream acoustic wave at the inlet (figures 4–7) because the wavelengths for entropy waves are much shorter than for acoustic waves. Hence the wavelength of the disturbances becomes comparable with nozzle dimensions at much lower frequencies. Formally, we require  $\Omega \ll \bar{M}$  for the analytical results to be valid (e.g. the small correction due to the effective length in (3.26) is  $O(\Omega/\bar{M})$ ). For the flow considered here this means  $\Omega \ll 0.17$ . We see in figures 8 and 9 that although the magnitude of our low-frequency asymptotic form is inaccurate once  $\Omega/(2\pi) \approx 0.15$ , the phase change and hence the nozzle effective length is accurate up to much higher frequencies.

### 5.1.3. Vorticity wave

For comparison with §3 we only consider the reflection coefficient for vorticity waves of the ‘first type’ (see (2.8)). The boundary condition used at  $x = 0$  was the same as for the case of an incident entropy wave except that we apply (2.8) with  $A_V$  a fixed constant and  $V(r) = B_n(r)$ . Now however the contribution of the vorticity wave to  $u'$  must be considered when finding  $A_+$  and  $A_-$ . The reflection coefficient is then  $\bar{c}k_-A_-/(n\alpha_-A_V)$  for the converged solution.

For  $n = 0$ , it can easily be seen from the linearized Euler equations that only  $w'$  will be non-zero in the nozzle, hence there is no reflected acoustic wave. The disturbance represents axisymmetric radial vorticity which remains uncoupled from the pressure field even when accelerating through a nozzle. Figure 10 shows results for  $n = 1$ . As in

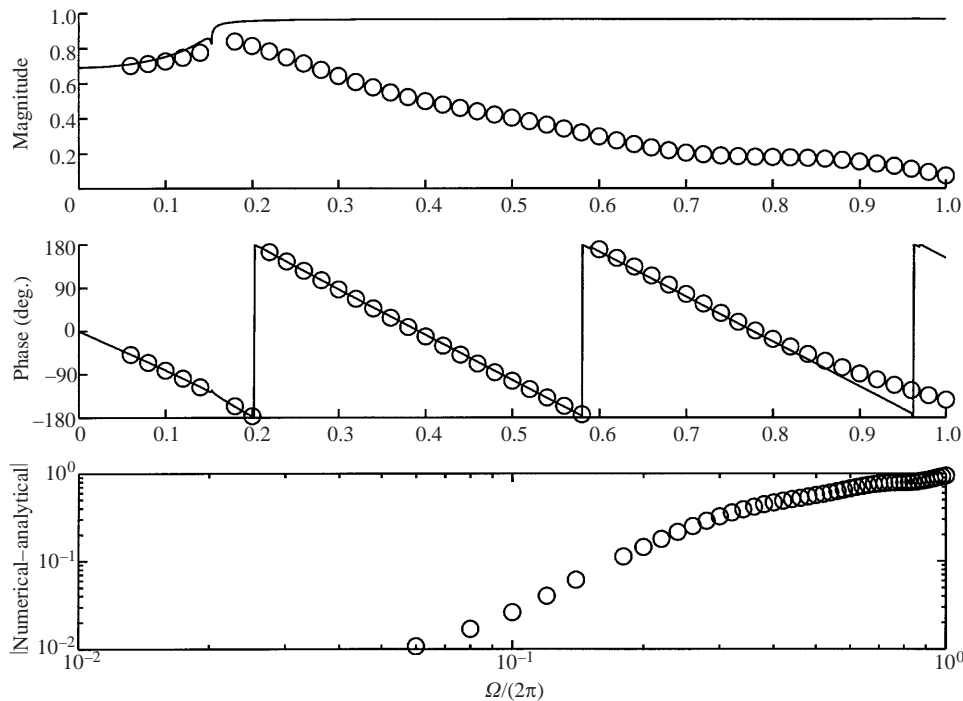


FIGURE 10. Magnitude and phase of the reflection coefficient for a choked nozzle with a vorticity wave at the inlet ( $n = 1$ ). The circles and solid lines denote numerical and analytical results respectively. The absolute difference between the numerical and analytical results is also shown.

figure 9, at low frequencies agreement between numerical results and the asymptotic analysis is good, but it becomes poor as the frequency increases. The wavelengths of vorticity waves are the same as for entropy waves (both are convected with the mean flow) and hence the explanation for this poor agreement is as described in the previous section.

### 5.2. Choked inlet nozzle

We now have a nozzle with no inlet disturbances and an acoustic wave propagating upstream towards its outlet. In contrast to the previous cases, here the mean flow downstream of the throat is important. In order for the flow perturbations downstream of the nozzle to be in the form of those in §2.1 we need the mean flow to be approximately uniform there. Hence in the following, a nozzle length of 0.4 m and an outlet pressure of 200 kPa were used on a grid of  $80 \times 20$  cells (see figure 3). This gives a more gradual expansion, reducing separation, and a weaker shock. For the perturbations, at each pseudo-time step  $p'$  and  $u' + nw'/(k_0 r)$  at  $x = x_{max}$  were used to find  $A_+$  and  $A_-$  in a similar way to the inlet boundary treatment for the downstream acoustic wave case in the choked outlet nozzle, described above. Here, by considering  $u' + nw'/(k_0 r)$  instead of  $u'$  we do not need to consider the vorticity and entropy waves (see (2.5)–(2.8)). Then  $p'$  and  $u' + nw'/(k_0 r)$  were recalculated using this value of  $A_-$  but setting  $A_+$  to be a fixed constant. This was used to reset  $p'$  and  $u'$  at  $x = x_{max}$  (using the original  $w'(x_{max}, r)$ ). As before higher-order radial modes were ignored. To allow entropy and vorticity waves to be present  $\rho'$ ,  $w'$  and  $v'$  were not recalculated at  $x = x_{max}$ . The reflection coefficient for the acoustic waves (i.e. the pressure reflection

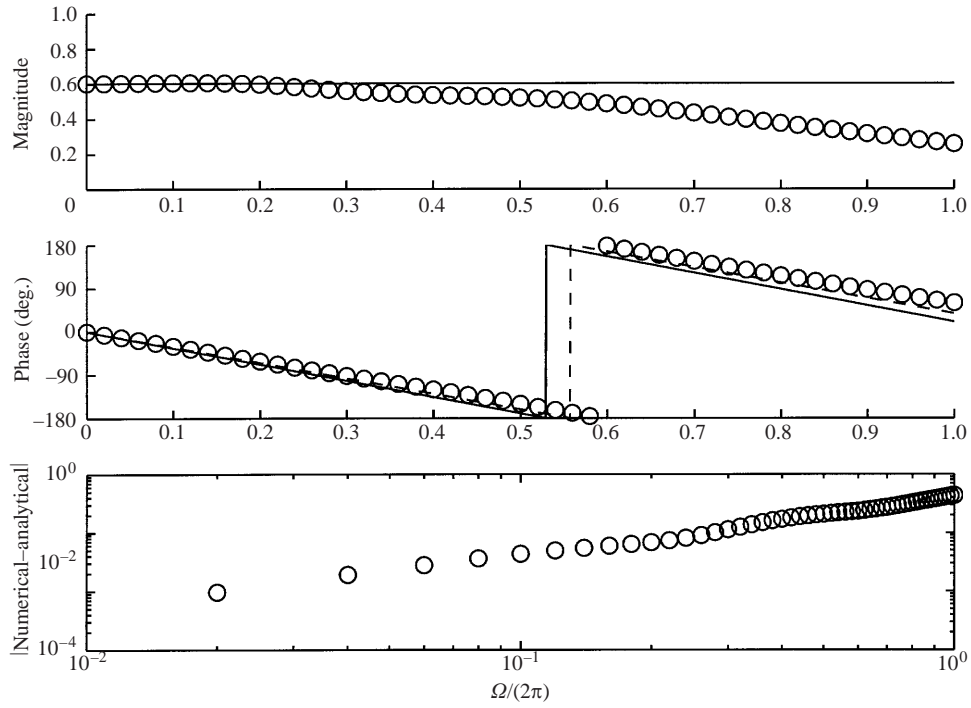


FIGURE 11. Magnitude and phase of the reflection coefficient for a choked nozzle with an upstream acoustic wave at the outlet ( $n = 0$ ). The circles denote numerical results. The solid and dashed lines represent analytical results (applied at the throat and approximate shock position, respectively). The absolute difference between the analytical result (applied at the throat) and the numerical results is also shown.

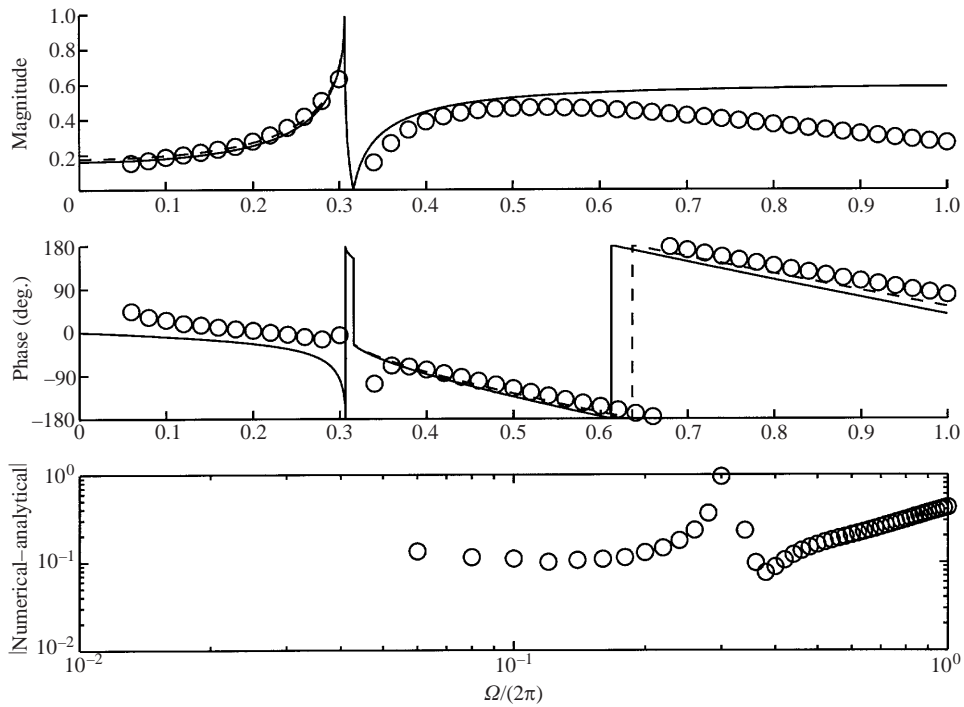


FIGURE 12. As figure 11 but for  $n = 1$ .

coefficient) is then given by  $A_+/A_-$  for the converged solution. As mentioned in §4 there should be no disturbances upstream of the shock, hence the inlet boundary conditions are applied at each pseudo-time step by setting all perturbations to zero at  $x = 0$ .

Numerical results for the reflection coefficient with  $n = 0$  are shown in figure 11. The solid and dashed lines represent the analytical result (4.14) applied at  $x = 0.2$  m (the throat) and  $x = 0.21$  m (approximately the shock position), respectively. (The absolute difference between the analytical result applied at  $x = 0.2$  m and the numerical results is also shown.) An effective length for the nozzle could be found in a way similar to that in §3. Figure 12 shows corresponding results for  $n = 1$ . As before, the cutoff frequency of the nozzle is 440 Hz but as  $x_{max} = 0.4$  m this is now equivalent to  $\Omega/(2\pi) = 0.31$ . In both figures we see that there is good agreement between the numerical results and analysis. Applying (4.14) at the shock gives a slightly better fit with the numerical results. As expected for a low-frequency asymptotic theory, agreement deteriorates at higher frequencies. For  $n = 1$  phase agreement is not as good below cutoff. It is thought that this is due to the cutoff waves being more sensitive to the non-uniformity in the mean flow. Results for  $n = 2$  (not shown) were similar, with phase agreement below cutoff being worse.

## 6. Conclusions

The reflection coefficient for a choked exit nozzle with either a downstream acoustic wave, entropy wave or vorticity wave present has been investigated both analytically and numerically. Although these three cases have been considered separately, the reflected acoustic wave created by a combination of these can be derived by superposition as the sum of the waves for the separate cases. An asymptotic analysis was conducted for low frequency. The results show that the boundary condition for a compact choked nozzle found by Marble & Candel may generally be applied even when circumferential modes are present. The solution was extended to second order in the compactness ratio and we showed that this correction may be expressed as an effective length, which was found to be the same for all waves (except for the acoustic wave near its cutoff frequency). This effective length is simply the mean velocity at the inlet multiplied by the convection time to the throat. The asymptotic analysis was found to give good agreement with the numerical calculations up to a non-dimensional frequency ( $\Omega/(2\pi)$ ) of 0.3 for the acoustic wave and 0.15 for the convected waves. This is as expected since the analysis becomes invalid when the wavelengths/ $(2\pi)$  become comparable with the nozzle dimensions. The analysis is suitable for application to combustion instabilities in gas turbines where this non-dimensional frequency is typically less than 0.1.

The reflected acoustic, entropy and vorticity waves created by an upstream acoustic wave in a choked inlet nozzle have also been found. It has been shown that the entropy perturbation produced is not negligible, even if the shock is weak and the following area increase is smooth. For circumferential modes, a vorticity wave is also created. The asymptotic analysis was again found to agree with the numerical results at low frequency.

This work was funded by the European Commission whose support is gratefully acknowledged. It is part of the GROWTH programme, research project ICLEAC: Instability Control of Low Emission Aero Engine Combustors (G4RD-CT2000-0215).

**Appendix. Cutoff frequencies for a narrow annular gap**

Writing  $b = a(1 + \epsilon)$ , we consider the values of  $\lambda_{n,m}$  for  $\epsilon \ll 1$ . The equation for  $\lambda_{n,m}$  can be written as

$$\frac{dJ_n}{dr}(\alpha) \frac{dY_n}{dr}(\alpha(1 + \epsilon)) - \frac{dJ_n}{dr}(\alpha(1 + \epsilon)) \frac{dY_n}{dr}(\alpha) = 0, \quad (\text{A } 1)$$

where  $\alpha = \lambda_{n,m}a$ . We first suppose that  $\alpha$  is order 1 and take  $\alpha = \alpha_0 + \alpha_1\epsilon + \alpha_2\epsilon^2 + O(\epsilon)^3$ . Substituting this into equation (A 1) and using Taylor expansions, the order- $\epsilon$  terms are

$$\alpha_0[J'_n(\alpha_0)Y''_n(\alpha_0) - J''_n(\alpha_0)Y'_n(\alpha_0)] = 0. \quad (\text{A } 2)$$

Replacing  $J''_n$  and  $Y''_n$  using Bessel's equation gives

$$\alpha_0(n^2/\alpha_0^2 - 1)[J'_n(\alpha_0)Y_n(\alpha_0) - J_n(\alpha_0)Y'_n(\alpha_0)] = 0. \quad (\text{A } 3)$$

Using the property  $J_n(z)Y'_n(z) - J'_n(z)Y_n(z) = 2/(\pi z)$  (see for example Abramowitz & Stegun 1965), we see that the only solution is  $\alpha_0 = n$ . Hence this must be the value corresponding to  $m = 0$ , and for  $m \geq 1$  the assumption that  $\alpha$  is order 1 must be incorrect. To find  $\alpha_1$  for the  $m = 0$  solution we consider the order- $\epsilon^2$  terms from (A 1), which are

$$\frac{1}{2}n(n + 2\alpha_1)[J'_n(n)Y'''_n(n) - J'''_n(n)Y'_n(n)] = 0. \quad (\text{A } 4)$$

Substituting for  $J'''_n$  and  $Y'''_n$  from the derivative of Bessel's equation and using the property quoted above it can be shown that  $J'_n(n)Y'''_n(n) - J'''_n(n)Y'_n(n) \neq 0$ , hence  $\alpha_1 = -\frac{1}{2}n$ . Therefore

$$\lambda_{n,0} = n/R + O(\epsilon)^2, \quad (\text{A } 5)$$

where  $R = \frac{1}{2}(a + b)$ . (Note however that this is only valid if  $n \ll \epsilon^{-1}$  otherwise the assumption that  $\alpha$  is order 1 is not satisfied.)

For  $m \geq 1$ ,  $\alpha$  must be larger than order 1. Using the properties

$$J'_n(z) = \sqrt{2/(\pi z)} \left( -\sin \chi - \frac{4n^2 + 3}{8z} \cos \chi + O(z^{-2}) \right), \quad (\text{A } 6a)$$

$$Y'_n(z) = \sqrt{2/(\pi z)} \left( \cos \chi - \frac{4n^2 + 3}{8z} \sin \chi + O(z^{-2}) \right), \quad (\text{A } 6b)$$

where  $\chi = z - \frac{1}{2}n\pi - \frac{1}{4}\pi$  (see for example Abramowitz & Stegun 1965), in (A 1) gives

$$-[2/(\pi\alpha)] \sin \alpha\epsilon + O(\alpha^{-3}) = 0 \quad (\text{A } 7)$$

(assuming that  $n^2 \ll \alpha$ ). Hence the solutions are  $\alpha\epsilon = \pi + O(\alpha^{-2}), 2\pi + O(\alpha^{-2}), \dots$  giving

$$\lambda_{n,m} = m\pi/(b - a) + O(\epsilon). \quad (\text{A } 8)$$

## REFERENCES

- ABRAMOWITZ, M. & STEGUN, I. A. (Eds.) 1965 *Handbook of Mathematical Functions*. Dover.  
 BATCHELOR, G. K. 1967 *An Introduction to Fluid Dynamics*. Cambridge University Press.  
 BLOXSIDGE, G. J., DOWLING, A. P. & LANGHORNE, P. J. 1988 Reheat buzz: an acoustically coupled combustion instability. Part 2. Theory. *J. Fluid Mech.* **193**, 445-473.  
 CROCCO, L. & SIRIGNANO, W. A. 1967 Behaviour of supercritical nozzles under three-dimensional oscillatory conditions. *AGARDograph* 117.

- CULICK, F. E. C. & ROGERS, T. 1983 The response of normal shocks in diffusers. *AIAA J.* **21**, 1382–1390.
- DENTON, J. D. 2002 The effects of lean and sweep on transonic fan performance. *Task Q.* **6**, 1–17.
- EVERSMAN, W. 1994 Theoretical models for duct acoustic propagation and radiation. In *Aeroacoustics of Flight Vehicles: Theory and Practice* (ed. H. H. Hubbard), vol. 2, chap. 13, pp. 101–163. Acoustical Society of America.
- KUO, C.-Y. & DOWLING, A. P. 1996 Oscillations of a moderately underexpanded choked jet impinging upon a flat plate. *J. Fluid Mech.* **315**, 267–291.
- MARBLE, F. E. & CANDEL, S. M. 1977 Acoustic disturbance from gas non-uniformities convected through a nozzle. *J. Sound Vib.* **55**, 225–243.
- SEUME, J. R., VORTMEYER, N., KRAUSE, W., HERMANN, J., HANTSCHK, C.-C., ZANGL, P., GLEIS, S., VORTMEYER, D. & ORTHMANN, A. 1997 Application of active combustion instability control to a heavy duty gas turbine. *ASME Paper 97-AA-119*.
- TYLER, J. M. & SOFRIN, T. G. 1962 Axial compressor noise studies. *SAE Trans.* **70**, 309–332.